COMPARING RELATIVE REACHABLE SETS ABOUT NEARLY CIRCULAR ORBITS

Jackson Kulik[*], Maxwell Zweig [†], and Dmitry Savransky [‡]

The relative reachable set problem considers the set of positions or states that are reachable at a given time under constraints on control authority. Some formulations of constraints on control authority lead to more analytically tractable computations of the reachable sets while others correspond more exactly to the constraints present in real-world spacecraft operations. We will compare different formulations of the relative reachable set problem and analyze the approximation quality of an impulsive reachable set as a stand-in for a constant-thrust reachable set and an energy-limited reachable set as a proxy for a thrust-limited reachable set.

INTRODUCTION

The relative reachable set problem examines the set of positions or combined position and velocity states relative to an uncontrolled trajectory that are accessible to a satellite at a given instant or interval in time. The relative reachable set problem is often characterized by smaller control authorities, time spans, and size of the reachable set than when considering absolute/inertial reachable sets. As such, using a linear approximation of the dynamics about the uncontrolled trajectory is typically appropriate. The relative reachable set problem lends itself well to the study of rendezvous and formation flight,[1] collision risk analysis,[2] as well as differential games.[3] In this work, we will not consider the envelope of a reachable set over an interval of time, but instead the reachable set at a given instant in time.

There are two main variants of the relative reachable set problem in terms of the formulation of the constraint on the control authority. The first variant considers the effects of a single, high-thrust maneuver approximated as an impulsive change in velocity or Δv.[1,2] In this work, we will expand upon the study of reachable sets under high-thrusts by considering the reachable set of a constant-thrust maneuver over a finite time period. This is a reasonable model for the execution of a variety of controls implemented in the formation flying and rendezvous setting, because trajectory optimization under the assumption of finite-time constant-thrust burns is of similar computational difficulty to optimization with impulsive burns while yielding more realistically implementable maneuvers.[4,5] Both of these formulations lead to ellipsoidal reachable sets, and obtaining the position only or full state reachable set is a simple computation. We will compare these reachable sets as the limit on the acceleration is changed or equivalently as the duration of the constant-thrust maneuver is varied. The other class of approaches to formulating the relative reachable set problem applies to the low-thrust setting in which neither of the two previous approaches work as an accurate model

[*]PhD Candidate, Center for Applied Mathematics, Cornell University, Ithaca, NY, 14850. jpk258@cornell.edu
[†]Undergraduate Researcher, Mathematics, Cornell University, Ithaca, NY, 14850.
[‡]Associate Professor, Mechanical and Aerospace Engineering, Cornell University, Ithaca, NY, 14850.

for maneuvers. The most analytically tractable low-thrust reachable set is the energy-limited reachable set, which is characterized by limiting the integral of the squared 2-norm of the acceleration from the spacecraft between some initial time and the time at which the reachable set is considered. Closed-form solutions for this energy-limited reachable set can be calculated as ellipsoids corresponding to some quadratic form.[6,7] More realistic constraints for low-thrust spacecraft are the thrust-limited[3,8] and additionally fuel-limited cases.[9,10] However, these higher-fidelity formulations of the low-thrust relative reachable set problem do not lead to reachable sets with ellipsoidal or other simple geometries. We will compare the analytically tractable, energy-limited, reachable set with the more realistic, thrust-limited, reachable set to understand in what ways the energy-limited reachable set succeeds or fails to approximate the thrust-limited reachable set.

Linear Approximation of the Dynamics

Given an autonomous dynamical system in $\mathbb{R}^n$, the state vector $\mathbf{x} \in \mathbb{R}^n$ evolves according to the system of ordinary differential equations

$$\frac{d}{dt}\mathbf{x} = \mathbf{F}(\mathbf{x}), \quad \mathbf{x}(0) = \mathbf{x}_0 \tag{1}$$

The flow map associated with the dynamical system in Eq. 1 is defined such that

$$\frac{d}{dt}\varphi_t(\mathbf{x}_0) = \mathbf{F}(\varphi_t(\mathbf{x}_0)), \quad \varphi_0(\mathbf{x}_0) = \mathbf{x}_0 \tag{2}$$

The Jacobian of the flow map is the state transition matrix (STM) $\mathbf{\Phi}(t_f, t_0)$ associated with a given flow starting at the reference state $\mathbf{x}_0$ from time t_0 to time t_f. Taking the first-order partial derivative of Eq. 2, exchanging the order of temporal and spatial derivatives (assuming $\mathbf{F}$ has continuous spatial derivatives) and applying the chain rule yields the n^2 first-order variational equations

$$\frac{d\mathbf{\Phi}(t_f, t_0)}{dt_f} = \frac{\partial \mathbf{F}(\mathbf{x})}{\partial \mathbf{x}}\mathbf{\Phi}(t_f, t_0), \quad \mathbf{\Phi}(t_0, t_0) = \mathbf{I}_n \tag{3}$$

where $\mathbf{I}_n$ is the n dimensional identity matrix.

The state transition matrix $\mathbf{\Phi}(t_f, t_0)$ associated with an uncontrolled reference trajectory with three-dimensional position $\mathbf{r}$ and velocity $\mathbf{v}$ between time t_0 and time t_f gives a linear approximation of how initial perturbations to the state $\delta\mathbf{x}_0 = [\delta\mathbf{r}_0^T, \delta\mathbf{v}_0^T]^T$ evolve into perturbations in the final state of the trajectory $\delta\mathbf{x}_f = [\delta\mathbf{r}_f^T, \delta\mathbf{v}_f^T]^T$.

$$\delta\mathbf{x}_f \approx \mathbf{\Phi}(t_f, t_0)\delta\mathbf{x}_0 \tag{4}$$

The Clohessy-Wiltshire equations[11] and Tschauner-Hempel equations/Yamanaka-Ankersen[12] state transition matrix give analytical forms for the STM in the rotating radial, in-track, cross-track frame (RIC) under the assumptions of two-body dynamics with circular and elliptical reference orbits, respectively. Under other assumptions for which the STM cannot be calculated analytically, it can be computed by numerically integrating the first-order variational equations associated with the dynamical system and reference trajectory from Eq. 3. In this work, the analytical techniques presented are valid for any dynamical system and associated STM. However, all examples will pertain directly to the Earth Centered Inertial (ECI) frame or RIC frame STM associated with a circular reference orbit in the two-body problem. The specifics of this STM are described below.

The position vector $\delta\mathbf{r}$ is written in radial, in-track, and cross-track coordinates as

$$\delta\mathbf{r} = \delta x\hat{\mathbf{r}} + \delta y\hat{\mathbf{s}} + \delta z\hat{\mathbf{w}} \tag{5}$$

where $\hat{\mathbf{r}}$ is defined as the direction from Earth center to reference orbit, $\hat{\mathbf{w}}$ is in the direction of the specific angular momentum of the reference orbit, and $\hat{\mathbf{s}} = \hat{\mathbf{w}} \times \hat{\mathbf{r}}$ completes the right-handed system. In the case of a circular reference orbit, $\hat{\mathbf{s}}$ corresponds to the direction of the velocity vector of the reference satellite. The RIC STM for circular orbits given by the Clohessy-Wiltshire equations is

$$\delta\mathbf{x}^{\text{RIC}} = \left[\delta x, \delta y, \delta z, \delta\dot{x}, \delta\dot{y}, \delta\dot{z}\right] \tag{6}$$

$$\delta\mathbf{x}_f^{\text{RIC}} = \mathbf{\Phi}^{\text{RIC}}(t_f, t_0)\delta\mathbf{x}_0^{\text{RIC}} \tag{7}$$

$$\mathbf{\Phi}^{\text{RIC}}(t_f, t_0) = \begin{bmatrix} 4-3c & 0 & 0 & s/n & 2/n-2c/n & 0 \\ -6n\Delta t+6s & 1 & 0 & -2/n+2c/n & 4s/n-3\Delta t & 0 \\ 0 & 0 & c & 0 & 0 & s/n \\ 3ns & 0 & 0 & c & 2s & 0 \\ -6n+6nc & 0 & 0 & -2s & -3+4c & 0 \\ 0 & 0 & -ns & 0 & 0 & c \end{bmatrix} \tag{8}$$

$$\mathbf{\Phi}^{\text{RIC}}(t_f, t_0) = \begin{bmatrix} \mathbf{\Phi}_{\mathbf{r}}^{\mathbf{r}} & \mathbf{\Phi}_{\mathbf{v}}^{\mathbf{r}} \\ \mathbf{\Phi}_{\mathbf{v}}^{\mathbf{r}} & \mathbf{\Phi}_{\mathbf{v}}^{\mathbf{v}} \end{bmatrix} \tag{9}$$

where $s = \sin(n\Delta t)$, $c = \cos(n\Delta t)$, and n is the mean motion of the reference orbit with units consistent with the spatial units from $\mathbf{x}$ and temporal units from t. Each block of $\mathbf{\Phi}(t_f, t_0)$ is a three by three matrix giving the sensitivity of the final state of the superscript variable listed (relative position or velocity), with respect to the initial state of the subscript variable listed. Note in the following sections that equations involving vectors and STMs will be assumed to use a consistent frame (RIC or ECI) within the equation unless otherwise explicitly listed. The ECI frame STM can be constructed by applying the linear transformation between ECI and RIC on either side of the RIC frame STM.[13] Let $\mathbf{M}_{\text{ECI}}^{\text{RIC}}(t)$ and $\mathbf{M}_{\text{RIC}}^{\text{ECI}}(t)$ denote the transformations from ECI to RIC and RIC to ECI, respectively, where the RIC frame is defined around the reference satellite at the epoch t. Then

$$\mathbf{\Phi}^{\text{ECI}}(t_f, t_0) = \mathbf{M}_{\text{RIC}}^{\text{ECI}}(t_f)\mathbf{\Phi}^{\text{RIC}}(t_f, t_0)\mathbf{M}_{\text{ECI}}^{\text{RIC}}(t_0) \tag{10}$$

The effect of a constant-thrust maneuver on a satellite can be characterized by solving the inhomogeneous system of differential equations associated with thrusted relative motion around some reference orbit.[4,5] We denote the input transition matrix (ITM)[14] by $\mathbf{\Gamma}(t_1, t_0)$, where the ITM is a 6×3 matrix giving the sensitivity of the state at time t_1 to the constant acceleration $\mathbf{a}$ over the entire time interval between t_0 and t_1:

$$\mathbf{\Gamma}(t_1, t_0) = \int_{t_0}^{t_1} \mathbf{\Phi}_{\mathbf{v}}(t_1, \tau)\mathrm{d}\tau \tag{11}$$

The effects on the state $\delta\mathbf{x}_f$ after a burn-coast maneuver can be obtained by multiplying the STM after the burn concludes and the ITM over the course of the burn with acceleration vector $\mathbf{a}$

$$\delta\mathbf{x}_f \approx \mathbf{\Phi}(t_f, t_1)\mathbf{\Gamma}(t_1, t_0)\mathbf{a} \tag{12}$$

The effects on position alone $\delta\mathbf{r}_f$, are given by taking the upper three by six partition of the STM $\mathbf{\Phi}^{\mathbf{r}}(t_f, t_1)$:

$$\delta\mathbf{r}_f \approx \mathbf{\Phi}^{\mathbf{r}}(t_f, t_1)\mathbf{\Gamma}(t_1, t_0)\mathbf{a} \tag{13}$$

When the acceleration $\mathbf{a}$ is fixed in the reference satellite RIC frame or ECI frame, then Eqs. 11-13 describe the effect on the satellite state in the same frame.

In the RIC frame with a circular reference orbit, the ITM is given by

$$\mathbf{\Gamma}^{\text{RIC}}_{\text{RIC}}(\Delta t) = \begin{bmatrix} \frac{1-c}{n^2} & \frac{2n\Delta t-2s}{n^2} & 0 \\ \frac{2(s-n\Delta t)}{n^2} & \frac{4-4c}{n^2} - \frac{3\Delta t^2}{2} & 0 \\ 0 & 0 & \frac{1-c}{n^2} \\ \frac{s}{n} & \frac{2-2c}{n} & 0 \\ \frac{2(c-1)}{n} & \frac{4s}{n} - 3\Delta t & 0 \\ 0 & 0 & \frac{s}{n} \end{bmatrix} \tag{14}$$

The effect on position at time t_f in the RIC frame from a centered RIC fixed burn–one that is fixed in the RIC frame over the time interval starting at $t_0 - \frac{\Delta t}{2}$ and ending at $t_0 + \frac{\Delta t}{2}$–is given by the matrix

$$\mathbf{\Phi}^{\mathbf{r}}_{\text{RIC}}\left(t_f, t_0 + \frac{\Delta t}{2}\right)\mathbf{\Gamma}^{\text{RIC}}_{\text{RIC}}\left(t_0 + \frac{\Delta t}{2}, t_0 - \frac{\Delta t}{2}\right) = \begin{bmatrix} \frac{2s_2s_f}{n^2} & \frac{2n\Delta t-4s_2c_f}{n^2} & 0 \\ \frac{4s_2c_f-2n\Delta t}{n^2} & \frac{8s_2s_f}{n^2} - 3\Delta t(t_f - t_0) & 0 \\ 0 & 0 & \frac{2s_2s_f}{n^2} \end{bmatrix} \tag{15}$$

where $s_f = \sin(n(t_f - t_0))$, $c_f = \cos(n(t_f - t_0))$, $s_2 = \sin\left(\frac{n\Delta t}{2}\right)$, and $c_2 = \cos\left(\frac{n\Delta t}{2}\right)$.

We also consider the effect of a constant acceleration fixed in the ECI frame on the RIC state of the vehicle. Here, we will formulate the effects of a burn that is specified at a given epoch in the RIC frame but will be executed as a fixed burn in the ECI frame such that the burn has the specified RIC frame acceleration at the designated epoch. Let $\mathbf{R}^{\text{ECI}}_{\text{RIC}}(t)$ denote the rotation transformation from three dimensional position or control acceleration vectors in the RIC frame to the ECI frame.

$$\mathbf{\Gamma}^{\text{RIC}}_{\text{ECI},+}(t_1, t_0) = \int_{t_0}^{t_1} \mathbf{\Phi}^{\text{RIC}}_{\mathbf{v}}(t_1, \tau)\mathbf{R}^{\text{RIC}}_{\text{ECI}}(\tau)\mathbf{R}^{\text{ECI}}_{\text{RIC}}(t_0)\mathrm{d}\tau \tag{16}$$

$$= \int_{t_0}^{t_1} \mathbf{\Phi}^{\text{RIC}}_{\mathbf{v}}(t_1, \tau)\mathbf{Q}_{\hat{\mathbf{c}}}(-n(\tau - t_0))\mathrm{d}\tau \tag{17}$$

where

$$\mathbf{Q}_{\hat{\mathbf{c}}}(\theta) = \begin{bmatrix} \cos(\theta) & -\sin(\theta) & 0 \\ \sin(\theta) & \cos(\theta) & 0 \\ 0 & 0 & 1 \end{bmatrix} \tag{18}$$

For a circular reference orbit, the ITM given an ECI fixed burn specified in the RIC frame at the initial epoch is given by

$$\mathbf{\Gamma}^{\text{RIC}}_{\text{ECI},+}(\Delta t) = \begin{bmatrix} \frac{3n\Delta ts+4c-4}{2n^2} & -\frac{3(n\Delta tc-s)}{2n^2} & 0 \\ \frac{3(n\Delta t-2s+n\Delta tc)}{n^2} & \frac{3n\Delta ts+5c-5}{n^2} & 0 \\ 0 & 0 & \frac{1-c}{n^2} \\ \frac{3}{2}\Delta tc - \frac{s}{2n} & \frac{3}{2}\Delta ts & 0 \\ -\frac{3(n\Delta ts+c-1)}{n} & 3\Delta tc - \frac{2s}{n} & 0 \\ 0 & 0 & \frac{s}{n} \end{bmatrix} \tag{19}$$

In order to understand the effects of a constant-thrust burn specified based on a RIC thrust vector at the center of the burn we form the following ITM

$$\mathbf{\Gamma}^{\text{RIC}}_{\text{ECI},*}(t_1,t_0) = \int_{t_0}^{t_1} \mathbf{\Phi}^{\text{RIC}}_{\mathbf{v}}(t_1,\tau)\mathbf{R}^{\text{RIC}}_{\text{ECI}}(\tau)\mathbf{R}^{\text{ECI}}_{\text{RIC}}((t_1-t_0)/2)\mathrm{d}\tau \tag{20}$$

$$= \int_{t_0}^{t_1} \mathbf{\Phi}^{\text{RIC}}_{\mathbf{v}}(t_1,\tau)\mathbf{Q}_{\hat{\mathbf{c}}}(-n(\tau-(t_1-t_0)/2))\mathrm{d}\tau \tag{21}$$

For a circular reference orbit, the ITM given an ECI fixed burn specified in the RIC frame at the halfway point epoch is given by

$$\mathbf{\Gamma}^{\text{RIC}}_{\text{ECI},*}(\Delta t) = \begin{bmatrix} -\frac{s_2(s-3n\Delta t)}{2n^2} & \frac{8s_2-(3n\Delta t+s)c_2}{2n^2} & 0 \\ -\frac{21s_2+\sin\left(\frac{3n\Delta t}{2}\right)-12n\Delta t c_2}{2n^2} & \frac{s_2 s}{n^2} & 0 \\ 0 & 0 & \frac{1-c}{n^2} \\ -\frac{(s-3n\Delta t)c_2}{2n} & \frac{s_2(3n\Delta t+s)}{2n} & 0 \\ \frac{s_2(s-3n\Delta t)}{n} & \frac{-11s_2+\sin\left(\frac{3n\Delta t}{2}\right)+6n\Delta t c_2}{2n} & 0 \\ 0 & 0 & \frac{s}{n} \end{bmatrix} \tag{22}$$

The effect on position at time t_f in the RIC frame from a centered ECI fixed burn starting at $t_0 - \frac{\Delta t}{2}$ and ending at $t_0 + \frac{\Delta t}{2}$ is given by the matrix

$$\mathbf{\Phi}^{\mathbf{r}}_{\text{RIC}}\left(t_f, t_0+\frac{\Delta t}{2}\right)\mathbf{\Gamma}^{\text{RIC}}_{\text{ECI},*}\left(t_0+\frac{\Delta t}{2}, t_0-\frac{\Delta t}{2}\right) = \begin{bmatrix} -\frac{(s-3\Delta tn)s_f}{2n^2} & \frac{8s_2-(3\Delta tn+s)c_f}{2n^2} & 0 \\ \frac{-(s-3\Delta tn)c_f-10s_2+3\Delta tnc_2}{n^2} & \frac{(3\Delta tn+s)s_f-6n(t_f-t_0)s_2}{n^2} & 0 \\ 0 & 0 & \frac{2s_2 s_f}{n^2} \end{bmatrix} \tag{23}$$

COMPARING IMPULSIVE AND CONSTANT-THRUST REACHABLE SETS

Using the state transition matrix, the position reachable set at time t_f resulting from an impulse at time t_0 is given by the set of relative position vectors $\delta\mathbf{r}_f$ at time t_f, which satisfy the constraint

$$\left\| \left(\mathbf{\Phi}^{\mathbf{r}}_{\mathbf{v}}(t_f,t_0)\right)^{-1}\delta\mathbf{r}_f \right\|_2 \leq \Delta v_{\max} \tag{24}$$

where $\mathbf{\Phi}^{\mathbf{r}}_{\mathbf{v}}(t_f,t_0)$ denotes the upper right block of the state transition matrix, which gives the sensitivity of the final position to initial velocity and $\Delta v_{\max}$ represents the maximum allowable control authority as an impulse at t_0. The above expression is valid when the matrix $\mathbf{\Phi}^{\mathbf{r}}_{\mathbf{v}}(t_f,t_0)$ is nonsingular which is true except at multiples of half periods (e.g. $1/2, 1, 3/2$... periods) and solutions of a transcendental equation once per orbit (e.g. around $1.4, 2.4$... periods). Otherwise, the linearized approximation of the reachable set collapses down to one (at full periods) or two dimensions rather than three dimensions.[15–17] The singular value decomposition may be employed to analyze the geometry of the resulting reachable set. The left singular vectors $\mathbf{u}_i$ multiplied by the singular values σ_i and the maximum delta-v, $\Delta v_{\max}$, give the semi-axes of the ellipsoid, and the right singular vectors $\mathbf{v}_i$ scaled by $\Delta v_{\max}$ give the controls which give rise to the semi-axes of the reachable set. This is the principle underlying the maximal stretching, Cauchy-Green strain tensor, or local Lyapunov exponent method for designing and understanding stationkeeping maneuvers.[18–20] Note that the frame of the STM is not specified in Eq. 24. The impulsive reachable set in ECI coordinates can be

obtained from the reachable set in RIC coordinates by applying the linear transformation $\mathbf{M}_{\text{RIC}}^{\text{ECI}}(t_f)$ to every vector in the impulsive RIC reachable set. On the other hand, the relationship between the reachable set from a thrust that is constant in the RIC frame versus a thrust that is constant in the ECI frame is less simple. However, the singular value decomposition of the matrix $\mathbf{\Phi}^{\mathbf{r}}(t_f, t_1)\mathbf{\Gamma}(t_1, t_0)$ gives the semi-axes of the ellipsoidal reachable set associated with a constant-thrust burn and coast maneuver in just the same way as for the impulsive reachable set.

In order to compare the impulsive and constant-thrust reachable sets for the same values of t_0 and t_f, but with varying values of the thrusting cutoff time t_1, we can leverage the analytical formulation of both reachable sets. In particular, we can try to understand the ratio of the distance from the origin to the two reachable sets along a given direction $\delta\hat{\mathbf{r}}_f$. First, note that the magnitude of the impulsive reachable set along $\delta\hat{\mathbf{r}}_f$ is given by

$$\|\mathbf{r}_f^{(I)}\|_2 = \frac{\Delta v_{\max}}{\left\| \left(\mathbf{\Phi}_{\mathbf{v}}^{\mathbf{r}}(t_f, t_0)\right)^{-1} \delta\hat{\mathbf{r}}_f \right\|_2} \tag{25}$$

Next, the magnitude of the constant-thrust reachable set along $\hat{\mathbf{r}}_f$ is given by

$$\|\delta\mathbf{r}_f^{(C)}\|_2 = \frac{u_{\max}}{\left\| \left(\mathbf{\Phi}^{\mathbf{r}}(t_f, t_1)\mathbf{\Gamma}(t_1, t_0)\right)^{-1} \delta\hat{\mathbf{r}}_f \right\|_2} \tag{26}$$

where $u_{\max}$ is the maximum possible acceleration of the constant-thrust. The square of the ratio of the constant-thrust reachable set to the impulsive reachable set is given as a generalized Rayleigh quotient

$$\rho^2(\hat{\mathbf{r}}_f; t_0, t_1, t_f) = \frac{\Delta v_{\max}^2}{u_{\max}^2} \frac{\delta\hat{\mathbf{r}}_f^T \left(\mathbf{\Phi}^{\mathbf{r}}(t_f, t_1)\mathbf{\Gamma}(t_1, t_0)\right)^{-T} \left(\mathbf{\Phi}^{\mathbf{r}}(t_f, t_1)\mathbf{\Gamma}(t_1, t_0)\right)^{-1} \delta\hat{\mathbf{r}}_f}{\delta\hat{\mathbf{r}}_f^T \left(\mathbf{\Phi}_{\mathbf{v}}^{\mathbf{r}}(t_f, t_0)\right)^{-T} \left(\mathbf{\Phi}_{\mathbf{v}}^{\mathbf{r}}(t_f, t_0)\right)^{-1} \delta\hat{\mathbf{r}}_f} \tag{27}$$

The method of Lagrange multipliers shows that $\rho^2(\delta\hat{\mathbf{r}}_f; t_0, t_1, t_f)$ and thus $\rho(\delta\hat{\mathbf{r}}_f; t_0, t_1, t_f)$ has constrained stationary points (under the unit ball constraint for $\delta\hat{\mathbf{r}}_f$) that are solutions of the generalized eigenvalue problem

$$\left(\mathbf{\Phi}^{\mathbf{r}}(t_f, t_1)\mathbf{\Gamma}(t_1, t_0)\right)^{-T} \left(\mathbf{\Phi}^{\mathbf{r}}(t_f, t_1)\mathbf{\Gamma}(t_1, t_0)\right)^{-1} \mathbf{y} = \gamma \left(\mathbf{\Phi}_{\mathbf{v}}^{\mathbf{r}}(t_f, t_0)\right)^{-T} \left(\mathbf{\Phi}_{\mathbf{v}}^{\mathbf{r}}(t_f, t_0)\right)^{-1} \mathbf{y} \tag{28}$$

where the eigenvalues γ_i and eigenvectors $\mathbf{y}_i$ are denoted as such to avoid confusion with costates and velocities. Given that the above matrix pencil (pair of matrices considered in a generalized eigenvalue problem) is symmetric positive semi-definite in both matrices, the generalized eigenvalue problem can be solved using a Hermitian solver and the eigenpairs $(\gamma_i, \mathbf{y}_i)$, while not necessarily orthogonal, are guaranteed to be real and the eigenvalues are guaranteed positive.[21] The directions at which the extrema of the ratios of the two reachable sets take place and the values of that ratio are given by the eigenvectors and the evaluation of $\rho(\delta\hat{\mathbf{r}}_f; t_0, t_1, t_f)$ at that eigenvector.

For ease of presentation and because of the simple oscillatory behavior of out-of-plane motion, we present analysis for the in-plane relative reachable sets associated with circular reference orbits. When comparing between the impulsive reachable set and a comparable constant-thrust reachable set satisfying $\Delta v_{\max} = u_{\max}\Delta t$, one might expect the impulsive control to be more efficient and to always lead to a larger reachable set than a comparable constant-thrust reachable set. However, the boundaries of the reachable sets often intersect and the ratio $\rho(\delta\hat{\mathbf{r}}_f; t_0, t_1, t_f)$ takes on values below

and above unity. In Fig. 1, impulsive and constant-thrust reachable sets–constant in the RIC or ECI frame, and either beginning at the impulse epoch or centered at the impulse epoch–are plotted for a nondimensional circular orbit with mean motion set to unity $n = 1$, control magnitude of unity $\Delta v_{\max} = 1$, and constant-thrust time of 0.25 periods (a potentially unrealistically long time period to emphasize differences in the reachable sets that would be difficult to see at lower thrust durations). For any other circular orbit of a different size or control magnitude, the reachable sets will be of the same shape and relative size. The impulsive reachable set is nearly 1-dimensional for the 1.4 revolution case which is a well-known consequence of the singularity of the upper right block of the state transition matrix around that time-of-flight.[17] It can be seen that the RIC frame centered constant-thrust reachable set is closest to the impulsive reachable set, with the centered ECI frame constant-thrust set, RIC frame uncentered constant-thrust set, and the ECI frame uncentered constant-thrust set increasingly less similar to the impulsive reachable set. These two time-of-flights demonstrate that there is no consistent trend describing in which direction the reachable set is larger–sometimes the radial extent is larger and in other cases the reachable set may be smaller in both in-track and radial extent, but cover regions in space that the impulsive set does not. In Fig. 2, we

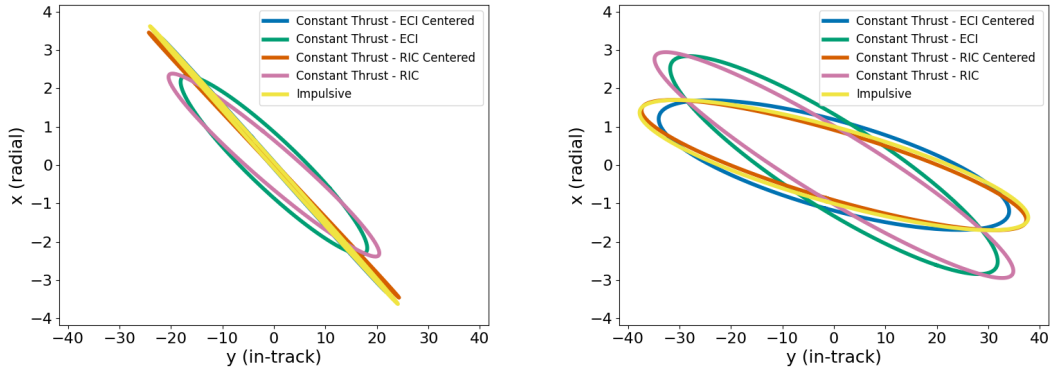

Figure 1: Unitless RRS for impulsive and constant-thrust controls. Time of flight is 1.4 periods on the left and 1.8 periods on the right.

plot the largest and smallest singular value/semi-axis length associated with the in-plane reachable sets of a circular reference orbit and impulsive or constant-thrust reachable sets using a thrust time of 0.05 periods (around 5 minutes for a LEO orbit). A linear trend with a sinusoidal forcing is clear in the larger singular value for all the reachable sets. On the other hand, the smaller singular value does not exhibit secular growth and goes to zero at the in-plane singular transfer times–at full periods and near 1.4 periods for the impulsive case, and near these values for the constant thrust cases. To emphasize the differences in the sizes of these reachable sets we plot the difference between the largest singular value associated with the constant-thrust reachable set and the largest singular value associated with the impulsive reachable set in Fig. 3. Additionally, the difference between the smallest singular values associated with the minimum distance of the constant-thrust and impulsive reachable sets is shown in Fig.3. The minimum singular values are almost the same visibly for the centered ECI and centered RIC constant-thrust maneuvers, as well as for the forward ECI and forward RIC maneuvers. One can see that the constant thrust maneuvers that are not centered at the impulsive maneuver epoch tend to have varying reachable set sizes. Sometimes the minimum extent of the forward constant-thrust reachable sets is larger than the smallest extent of the impulsive reachable set, and sometimes it is larger. On the other hand, the centered constant-thrust

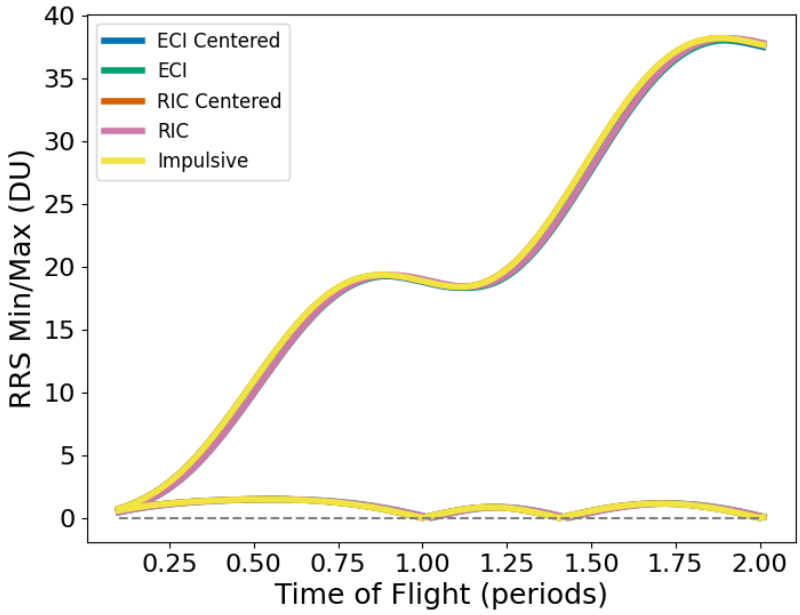

Figure 2: Singular values associated with in-plane minimum and maximum reachable set distances.

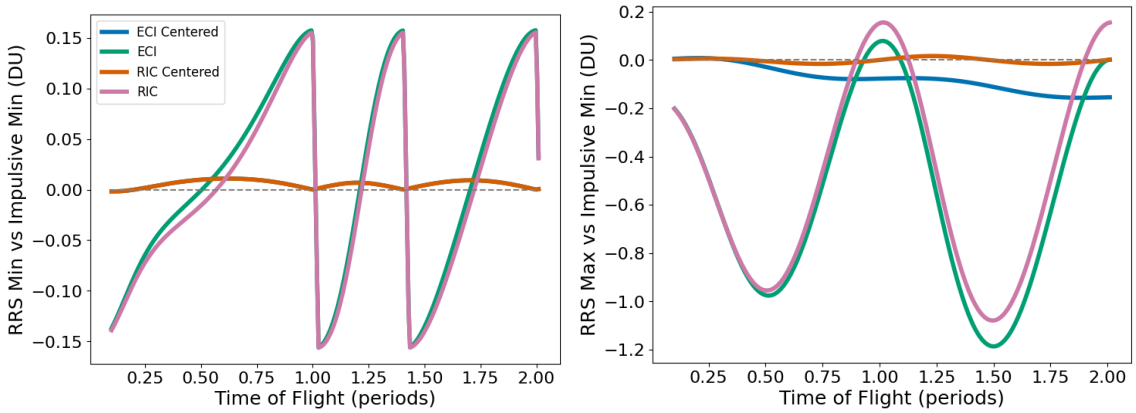

Figure 3: Difference between smallest (left) and largest (right) singular value for constant-thrust RRS vs impulsive RRS.

maneuvers have a slightly larger minimum extent than the impulsive reachable set except for a short period of time following the maneuver. When examining the maximum extent of the reachable sets, it is evident that the centered RIC constant-thrust reachable set has the most similar extent as the impulsive reachable set. On the other hand, the centered ECI constant-thrust reachable set tends to have a smaller maximum extent as compared with the impulsive reachable set. This difference in the maximum extent of the two reachable sets grows over time. So far, we have compared individually the extent of the reachable sets, but have not compared them along the same directions. For example, the maximum extent of one reachable set may be in a very different direction than another reachable set with a similar maximum extent.

In Fig. 4, the minimum and maximum ratios between the impulsive reachable set and various constant-thrust reachable sets are displayed. Near singular transfer times at 1, 2, and around 1.4 revolutions, the ratios limit to infinity and zero for each of the reachable sets. The uncentered constant-thrust reachable sets exhibit generally higher maximum ratios relative to the impulsive reachable set and lower minimum ratios when compared to the centered constant-thrust burns. This indicates that generally these constant-thrust reachable sets where the thrust begins at the impulse epoch are more distinct from the corresponding impulsive reachable set as compared with a centered constant-thrust maneuver reachable set. For short time-of-flight, the forward constant-thrust reachable sets are a subset of the impulsive reachable set, while they are generally neither a superset nor a subset (having some overlap) after around a quarter of a revolution in the case of this 0.05 period thrust time. The behavior of the centered constant-thrust reachable sets is examined more closely in Fig. 5. We see that the maximum and minimum ratios of the ECI fixed centered constant-thrust reachable set are nearly constant regardless of the time-of-flight (except near the singular transfer times where the ratios blow up or go to zero) for a relatively small thrust-time like is shown in this example. On the other hand, there is more variation in the ratios of the RIC fixed centered constant-thrust reachable set. The RIC reachable set generally has a minimum ratio relative to the impulsive reachable set that is smaller than the minimum ratio for the impulsive reachable set (though they are quite similar far away from the singular transfer times). However, the maximum ratio of the RIC centered constant-thrust reachable set it generally smaller than the ECI centered constant-thrust reachable set. This indicates that the impulsive and RIC centered constant-thrust reachable sets are generally more similar than the ECI centered constant-thrust reachable set and the impulsive reachable set. Except for a small period of time near three quarters of a period where the RIC centered constant-thrust reachable set is a subset of the impulsive reachable set, neither centered constant-thrust reachable strictly contains or is contained by the impulsive reachable set.

One implication of this study is that a RIC centered constant-thrust maneuver is, in some sense, more similar in its effects to an impulsive maneuver than an ECI centered constant-thrust maneuver. On the other hand, an ECI centered constant-thrust maneuver may sometimes be more efficient for reaching a given point than the corresponding RIC centered constant-thrust maneuver to reach that point, though this will depend on exactly the desired effect to be achieved from the control.

COMPARING THE ENERGY-LIMITED AND THRUST-LIMITED REACHABLE SETS

In describing energy-limited and thrust-limited reachable sets, we must first define the respective optimal control problems. In both cases, the original dynamics model from Eq. 1 is augmented with a control acceleration given by the vector $\mathbf{u}$.

$$\frac{d\mathbf{x}}{dt} = \mathbf{F}(\mathbf{x}) + \begin{bmatrix} 0 \\ \mathbf{u} \end{bmatrix} \tag{29}$$

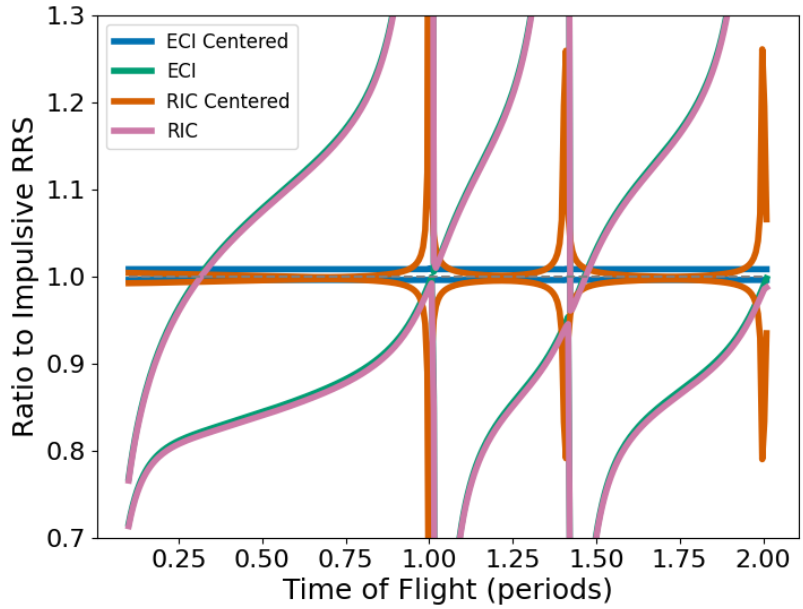

Figure 4: The minimum and maximum ratios of the in-plane constant-thrust reachable sets with respect to the impulsive reachable sets.

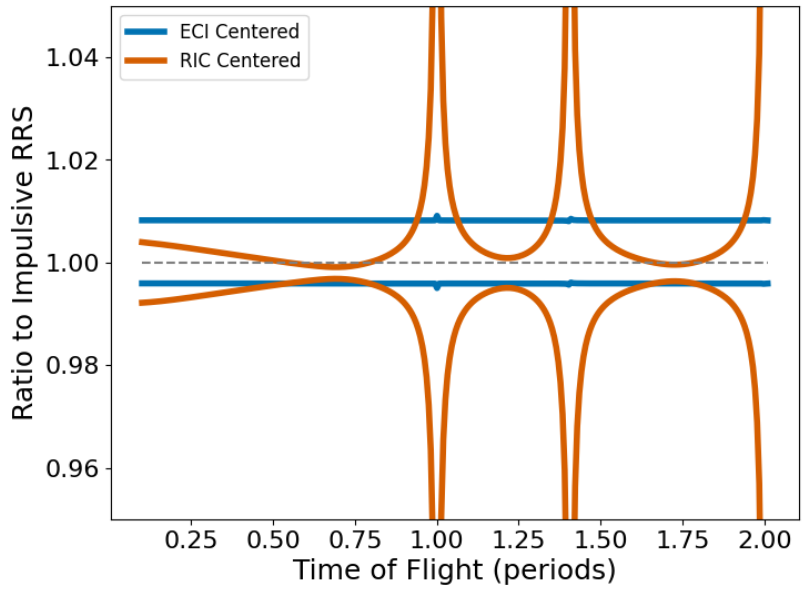

Figure 5: The minimum and maximum ratios of the in-plane ECI-centered constant-thrust reachable set with respect to the impulsive reachable sets.

Energy-limited Reachable Set

We begin by describing energy optimal control of a satellite relative to an arbitrary reference trajectory. The energy cost of some control profile is given by the integral of the squared acceleration

$$E = \int_{t_0}^{t_f} ||\mathbf{u}||^2 dt \tag{30}$$

Optimal control from one state to another in a proscribed time interval t_0 to t_f under the proscribed cost function in Eq. 30 is given by solving a two-point boundary value problem associated with a system of ordinary differential equations. This approach invokes the Pontryagin Maximal Principle (PMP) and is also known as indirect optimal control. The differential equations for the indirect optimal control problem have twice as many dimensions as the state of the original system:

$$\frac{d\mathbf{x}}{dt} = \mathbf{F}(\mathbf{x}) + \begin{bmatrix} 0 \\ \mathbf{u} \end{bmatrix} \tag{31}$$

$$\frac{d\boldsymbol{\lambda}}{dt} = -\left(\frac{\partial \mathbf{F}(\mathbf{x})}{\partial \mathbf{x}}\right)^T \boldsymbol{\lambda} \tag{32}$$

$$\mathbf{u} = -\boldsymbol{\lambda}_\mathbf{v} \tag{33}$$

where $\boldsymbol{\lambda}_\mathbf{v}$ is the velocity costate vector consisting of the last three elements of the costate vector $\boldsymbol{\lambda}$.[22] The energy cost E for some optimal control can then be written as an integral in terms of these velocity costates whose evolution is described by the ordinary differential equations in Eq. 32

$$E = \int_{t_0}^{t_f} \boldsymbol{\lambda}_\mathbf{v}^T \boldsymbol{\lambda}_\mathbf{v} dt \tag{34}$$

Finding an energy optimal trajectory becomes a problem of finding the initial costate vector that solves the two point boundary value problem associated with reaching the desired terminal state. The above derivation is independent of any sort of linearization assumption. To solve this problem generally, numerical solution of the boundary value problem with shooting or collocation is typically required. However, if the optimal control takes place near some reference trajectory, the state transition matrix of the augmented system may be used to provide linear approximations to the initial costate solutions, control vector over time, and a quadratic approximation of the overall cost. The following derivation of that quadratic energy cost approximation is equivalent to the one described in Lee et. al.[6] Defining the augmented state vector as

$$\mathbf{y} = \begin{bmatrix} \mathbf{x} \\ \boldsymbol{\lambda} \end{bmatrix} = \begin{bmatrix} \mathbf{r} \\ \mathbf{v} \\ \boldsymbol{\lambda}_\mathbf{r} \\ \boldsymbol{\lambda}_\mathbf{v} \end{bmatrix} \tag{35}$$

the state transition matrix associated with the augmented dynamical system from Eqs. 31-33 about a natural (without control) reference trajectory beginning at state $\mathbf{x}_0$ will also be denoted as $\boldsymbol{\Phi}_\mathbf{y}^\mathbf{y}(t_f, t_0)$. This state transition matrix for the augmented system maps perturbations $\delta\mathbf{y}_0$ from a natural reference trajectory at time t_0

$$\mathbf{y}_0 = [\mathbf{x}_0^T \quad \mathbf{0}^T]^T \tag{36}$$

into a linear approximation of the final perturbations to the augmented state at time t_f:

$$\delta\mathbf{y}_f \approx \boldsymbol{\Phi}_\mathbf{y}^\mathbf{y}(t_f, t_0)\delta\mathbf{y_0} \tag{37}$$

where $\boldsymbol{\Phi}_\mathbf{y}^\mathbf{y}(t_f, t_0)$ can be partitioned into blocks

$$\boldsymbol{\Phi}_\mathbf{b}^\mathbf{a}(t_f, t_0) = \frac{\partial \mathbf{a}_f}{\partial \mathbf{b}_0} \tag{38}$$

where $\mathbf{a}, \mathbf{b}$ are any of the vectors comprising the augmented state such as $\mathbf{y}, \mathbf{x}, \mathbf{r}, \mathbf{v}, \boldsymbol{\lambda}, \boldsymbol{\lambda}_\mathbf{r}, \boldsymbol{\lambda}_\mathbf{v}$. Using the definition of these blocks of the state transition matrix associated with the augmented system dynamics around a natural reference trajectory, the linearized boundary value problem to move from the reference orbit at the initial time ($\delta\mathbf{x}_0 = 0$) to some arbitrary close state $\delta\mathbf{x}_f$ at the final time t_f is solved by finding the initial costate vector deviation

$$\delta\boldsymbol{\lambda}_0 \approx \left(\boldsymbol{\Phi}^{\mathbf{x}}_{\boldsymbol{\lambda}}(t_f, t_0)\right)^{-1} \delta\mathbf{x}_f \tag{39}$$

Given the zero initial state deviation, the velocity costate at an arbitrary time can be written as

$$\boldsymbol{\lambda}_\mathbf{v}(t) \approx \boldsymbol{\Phi}^{\boldsymbol{\lambda}_\mathbf{v}}_{\boldsymbol{\lambda}}(t, t_0)\delta\boldsymbol{\lambda}_0 = \boldsymbol{\Phi}^{\boldsymbol{\lambda}_\mathbf{v}}_{\boldsymbol{\lambda}}(t, t_0)\left(\boldsymbol{\Phi}^{\mathbf{x}}_{\boldsymbol{\lambda}}(t_f, t_0)\right)^{-1} \delta\mathbf{x}_f \tag{40}$$

Rewriting the energy cost function from Eq. 30, we arrive at a quadratic approximation of the energy using the linearized dynamics around a natural reference trajectory

$$E = \delta\mathbf{x}_f^T \underbrace{\left(\boldsymbol{\Phi}^{\mathbf{x}}_{\boldsymbol{\lambda}}(t_f, t_0)\right)^{-T} \left(\int_{t_0}^{t_f} \left(\boldsymbol{\Phi}^{\boldsymbol{\lambda}_\mathbf{v}}_{\boldsymbol{\lambda}}(t, t_0)\right)^T \boldsymbol{\Phi}^{\boldsymbol{\lambda}_\mathbf{v}}_{\boldsymbol{\lambda}}(t, t_0) dt\right) \left(\boldsymbol{\Phi}^{\mathbf{x}}_{\boldsymbol{\lambda}}(t_f, t_0)\right)^{-1}}_{\mathbf{E}} \delta\mathbf{x}_f \tag{41}$$

The energy-limited reachable set under linearized dynamics is given by the set of final state perturbations $\delta\mathbf{x}_f$ such that the following quadratic form is less than some maximum value

$$\delta\mathbf{x}_f^T \mathbf{E} \delta\mathbf{x}_f \leq E_{\text{max}} \tag{42}$$

The semi-axes of the energy-limited reachable set in the full six-dimensional state space are given by

$$\boldsymbol{\alpha}_i = \sqrt{\frac{E_{\text{max}}}{\gamma_i}} \mathbf{y}_i \tag{43}$$

where $(\mathbf{y}_i, \gamma_i)$ is an eigenpair of the matrix $\mathbf{E}$. While the energy-limited reachable set has been studied extensively, analytical statements have focused mainly on the full state reachable set rather than the position only reachable set. We note here that the semi-axes of the ellipsoid for the position reachable set can be obtained through a generalized eigenvalue problem derived from the method of Lagrange multipliers applied to the following constrained optimization problem

$$\max_{\delta\mathbf{x}_f^T \mathbf{E} \delta\mathbf{x}_f = E_{\text{max}}} \delta\mathbf{r}_f^T \delta\mathbf{r}_f = \max_{\delta\mathbf{x}_f^T \mathbf{E} \delta\mathbf{x}_f = E_{\text{max}}} \delta\mathbf{x}_f^T \begin{bmatrix} \mathbf{I}_3 & \mathbf{0}_3 \\ \mathbf{0}_3 & \mathbf{0}_3 \end{bmatrix} \delta\mathbf{x}_f \tag{44}$$

The resulting generalized eigenvalue problem with three nonzero eigenvalues is

$$\mathbf{E}\mathbf{y} = \gamma \begin{bmatrix} \mathbf{I}_3 & \mathbf{0}_3 \\ \mathbf{0}_3 & \mathbf{0}_3 \end{bmatrix} \mathbf{y} \tag{45}$$

where the semi-axes of the position energy-limited reachable set are then given by

$$\boldsymbol{\alpha}_i^\mathbf{r} = \sqrt{\frac{E_{\text{max}}}{\gamma_i}} \mathbf{y}_i^\mathbf{r} \tag{46}$$

where $\mathbf{y}_i^\mathbf{r}$ denoted the position components of the eigenvector $\mathbf{y}_i$. Given the symmetry of the generalized eigenvalue problem, the generalized eigenvectors are orthogonal with respect to the matrix

on the right hand side of Eq. 45, and thus each of the position components of the eigenvectors $\mathbf{y}_i^{\mathbf{r}}$ are mutually orthogonal.[21] This proves that the position reachable set is also an ellipsoid. Note that the eigenpairs discussed for this matrix pencil in Eq. 45 are different from those associated with the matrix $\mathbf{E}$ alone. Further, note that the position reachable set described here cannot be calculated by taking the eigendecomposition of the upper left three by three block of the matrix $\mathbf{E}$, denoted as $\mathbf{E_{rr}}$. While the eigenvectors of Eq. 45 give information about the reachable set **projected** into the position only subspace, the eigenvectors of $\mathbf{E_{rr}}$ would give information about the reachable set **subject to the constraint** that the satellite arrives at its terminal condition with zero relative velocity (a subset of the overall position reachable set).

The maximum projection of the position along a given direction $\delta\hat{\mathbf{r}}_f$ within the reachable set can be obtained by a similar optimization yielding a generalized eigenvalue problem in terms of the outer product of that unit vector with itself. The resulting eigenvalue problem has only one nonzero eigenvalue due to the rank one matrix appearing on the right hand side:

$$\mathbf{E}\mathbf{y} = \gamma \begin{bmatrix} \delta\hat{\mathbf{r}}_f \delta\hat{\mathbf{r}}_f^T & \mathbf{0}_3 \\ \mathbf{0}_3 & \mathbf{0}_3 \end{bmatrix} \mathbf{y} \tag{47}$$

The maximum projected distance of the reachable set from the origin in the direction $\delta\hat{\mathbf{r}}_f$ is then given by

$$\sqrt{\frac{E_{\max}}{\gamma}} \tag{48}$$

for the one nonzero eigenvalue γ, where this eigenvalue is again different from those discussed above.

However, the maximum projection of the reachable set onto a given direction will not generally be the magnitude of the vector on the reachable set in that direction. In order to calculate the distance from the origin of the position reachable set in a given direction, forming the quadratic form associated with the position reachable set is expedient. Let

$$\mathbf{E}^* = \sum_{i=1}^{3} \gamma_i \mathbf{y}_i^{\mathbf{r}} (\mathbf{y}_i^{\mathbf{r}})^T \tag{49}$$

where γ_i and $\mathbf{y}_i$ are generalized eigenpairs coming from Eq. 45 and $\mathbf{y}_i^{\mathbf{r}}$ again denotes the vector consisting of the first three components of $\mathbf{y}_i$. The magnitude of the energy-limited position reachable set in the direction of $\delta\hat{\mathbf{r}}_f$ is given by

$$\|\delta\mathbf{r}_f\|_2 = \sqrt{\frac{E_{\max}}{\delta\hat{\mathbf{r}}_f^T \mathbf{E}^* \delta\hat{\mathbf{r}}_f}} \tag{50}$$

This efficient linear algebraic method for calculating the range of the reachable set in a particular direction allows us to compare the energy-limited reachable set and thrust-limited reachable set along a particular direction.

Thrust-Limited Reachable Set

For fuel-optimal control (neglecting mass loss over time) of a satellite relative to an arbitrary reference trajectory, the fuel cost for some control profile $\mathbf{u}$ is given by

$$J = \int_{t_0}^{t_f} ||\mathbf{u}|| dt \tag{51}$$

Relative to the energy-limited low-thrust case, computation of the more realistic thrust-limited case is intense: Due to the non-quadratic nature of the thrust constraint, the thrust-limited relative-reachable-set (RRS) is non-ellipsoidal and does not lend itself to as direct an analytical description as the energy-limited case. As in the energy-limited case, thrust-limited optimal controls can be found via application of the PMP to a system following the dynamics given by Eq. 31, however with a different set of constraints.

Choosing $\boldsymbol{\delta}$ as an arbitrary vector on the unit-sphere along which the final position is to be maximized, Gong et al.[3] show that for any initial state on the reference trajectory, finding the boundary of the thrust-limited RRS can be performed by solving the following fixed-time optimal control problem:

$$\begin{aligned} \text{maximize} \quad & \boldsymbol{\delta} \cdot \delta\mathbf{r}(t_f) \\ \text{subject to} \quad & \left[\delta\mathbf{r}, \delta\mathbf{v}\right]^T(t_0) = \mathbf{0}, \quad ||\mathbf{u}(t)|| \leq T_{\max}, \\ & \frac{d\mathbf{x}}{dt} = \mathbf{F}(\mathbf{x}) + \begin{bmatrix} 0 \\ \mathbf{u} \end{bmatrix}, \quad \boldsymbol{\delta} \times \delta\mathbf{r}(t_f) = \mathbf{0} \end{aligned} \tag{52}$$

Gong et al. show that due to convexity properties of the RRS, the constraint $\boldsymbol{\delta} \times \mathbf{r}(t_f) = \mathbf{0}$ can be relaxed, simplifying the control problem and allowing for the analysis given below. Though relaxing this constraint increases the tractability of the optimization, the resulting position vector on the reachable envelope may no longer point in the same direction as $\boldsymbol{\delta}$.

Invoking the PMP yields the same state and co-state differential equations as in the energy-limited case (Eqs. 31-32), however application of the constraint $||\mathbf{u}(t)|| \leq T_{\max}$ results in a different expression for the control authority $\mathbf{u}$ in terms of the co-states. As a direct result of the the thrust-limited constraint, the control $\mathbf{u}(t)$ that maximizes the Hamiltonian in the thrust-limited case is instead such that $\mathbf{u}$ is in the direction of the velocity co-state vector with magnitude equal to $T_{\max}$:

$$\mathbf{u} = \frac{\boldsymbol{\lambda}_{\boldsymbol{v}}(t)}{||\boldsymbol{\lambda}_{\boldsymbol{v}}(t)||} T_{\max} \tag{53}$$

The thrust-limited co-state dynamics are as given in Eq. 32 but subject to the boundary condition

$$\boldsymbol{\lambda}_f = \left[\mathbf{0}, \boldsymbol{\delta}\right]^T \tag{54}$$

As a direct result of the relationship between the state transition matrix and the adjoint system, the solution to the co-state equations can be expressed in the form

$$\boldsymbol{\lambda}(t) = \begin{bmatrix} \boldsymbol{\Phi}^{\mathbf{r}}_{\mathbf{r}}(t_f, t)^T \boldsymbol{\delta} \\ \boldsymbol{\Phi}^{\mathbf{r}}_{\mathbf{v}}(t_f, t)^T \boldsymbol{\delta} \end{bmatrix} \tag{55}$$

It is well known that for a general linear dynamical system with control vector $\mathbf{u}$, state transition matrix $\boldsymbol{\Phi}$, initial state $\mathbf{x}(t_0)$, and control response $\mathbf{B}(t)$, the solution to the system $\mathbf{x}(t)$ is given by:

$$\mathbf{x}(t) = \boldsymbol{\Phi}(t, t_0)\mathbf{x}(t_0) + \int_{t_0}^{t} \boldsymbol{\Phi}(t, \tau)\mathbf{B}(\tau)\mathbf{u}(\tau)d\tau \tag{56}$$

As a result, points in the direction $\delta\mathbf{r}_f$ on the boundary of the thrust-limited RRS can be found by substituting Eqs. 53 and 55 into Eq. 56 and then setting $\delta\mathbf{r}(t_0) = \mathbf{0}$ and $\delta\mathbf{v}(t_0) = \mathbf{0}$ as specified by the optimization constraints given in 52 :

$$\delta\mathbf{r}_f = \int_{t_0}^{t_f} T_{\max} \frac{\boldsymbol{\Phi}^{\mathbf{r}}_{\mathbf{v}}(t_f, t)\boldsymbol{\Phi}^{\mathbf{r}}_{\mathbf{v}}(t_f, t)^T \boldsymbol{\delta}}{\sqrt{\boldsymbol{\delta}^T \boldsymbol{\Phi}^{\mathbf{r}}_{\mathbf{v}}(t_f, t)\boldsymbol{\Phi}^{\mathbf{r}}_{\mathbf{v}}(t_f, t)^T \boldsymbol{\delta}}} dt \tag{57}$$

We note that the initial constraint given in Gong et al. can be relaxed to yield the RRS from any arbitrary starting state though we will only use initial states at the reference trajectory for analysis in this work. In this case, for $\delta\mathbf{x}(t_0) = \left[\delta\mathbf{r}_0, \delta\mathbf{v}_0\right]$, a point on the boundary of the thrust-limited RRS is given by:

$$\delta\mathbf{r}_f = \mathbf{\Phi}^{\mathbf{r}}_{\mathbf{r}}\delta\mathbf{r}(t_0) + \mathbf{\Phi}^{\mathbf{r}}_{\mathbf{v}}\delta\mathbf{v}_0 + \int_{t_0}^{t_f} T_{\max}\frac{\mathbf{\Phi}^{\mathbf{r}}_{\mathbf{v}}(t_f,t)\mathbf{\Phi}^{\mathbf{r}}_{\mathbf{v}}(t_f,t)^T\boldsymbol{\delta}}{\sqrt{\boldsymbol{\delta}^T\mathbf{\Phi}^{\mathbf{r}}_{\mathbf{v}}(t_f,t)\mathbf{\Phi}^{\mathbf{r}}_{\mathbf{v}}(t_f,t)^T\boldsymbol{\delta}}}dt \tag{58}$$

We compute the final RRS by uniformly sampling vectors on the unit circle and then mapping them through the relation given by Eq. 57.

Comparison Analysis

As in the impulsive and constant-thrust cases, we present analysis for the in-plane relative reachable sets associated with circular reference orbits. In the energy and fuel-limited case, a reasonable energy-limit for comparison with a maximum thrust $T_{\max}$ and time-of-flight Δt is $E_{\max} = T^2_{\max}\Delta t$. For this choice of $E_{\max}$, the energy-constrained reachable set will be a super-set of the thrust-constrained low-thrust reachable set for any terminal time or initial condition.

To put upper and lower bounds on the extent to which the comparable energy-limited reachable set over-approximates the thrust-limited reachable set in any direction for a given terminal time, we computed the thrust-limited RRS using the procedure described above, yielding a set of points on the boundary of the thrust-limited reachable set. Next, using the energy-limited procedure outlined above, we computed the reachable set associated with the energy $E_{\max} = T^2_{\max}\Delta t$ and initial condition $\delta\mathbf{x}(t_0) = \mathbf{0}$. Finally, for a given vector $\delta\mathbf{r}_f$ on the thrust-limited reachable set, the ratio between the energy-limited reachable set in the direction of $\delta\mathbf{r}_f$ and the thrust-limited reachable set $\delta\mathbf{r}_f$ is then given by

$$\frac{||\delta\mathbf{r}^E_f||}{||\delta\mathbf{r}_f||} = \frac{E_{\max}}{\sqrt{\delta\hat{\mathbf{r}}_f\boldsymbol{E}^*\delta\hat{\mathbf{r}}_f}\,\|\delta\mathbf{r}_f\|} \tag{59}$$

where $\delta\hat{\mathbf{r}}_f$ denotes the unit vector in the direction of $\delta\mathbf{r}_f$. Using this procedure, we analyzed how the minimum and maximum ratios between the RRS changed as terminal time changed, and also analyzed how the directions in which these minimum and maximum ratios changed over time. We set the constants $\mu = 3.986 \times 10^{14}\,\frac{\mathrm{m}^3}{\mathrm{s}^2}$ and $\alpha = 7,780\,\mathrm{km}$ yielding the mean-motion value of $n = 0.00092\,\mathrm{s}^{-1}$. We note that the minimum and maximum ratios between the thrust and impulsive limited RRS as function of time of flight will be invariant of the mean motion when time of flight is given in periods. For maneuvers lasting seconds to several minutes, we found that the comparable energy limited reachable set over-approximates the fuel-limited reachable set by approximately 15 percent, and that the degree of over-approximation as a function of direction remained close to uniform over this time period, as illustrated in Fig. 6. The over-approximation becomes less uniform for longer time-of-flights such as at half and full periods as seen in Fig. 7 and Fig. 8. Figs. 9-10 show plots of metrics associated with the differences in the energy and thrust-limited RRS over time. In Fig. 9, we show the angles (measured counterclockwise from the positive in-track axis such that in-track is 0 radians and positive radial is $\pi/2$ radians) at which the minimum and maximum ratios between the relative reachable sets occur, and how they vary over the course of a full orbital period under the orbital parameters chosen above. In Fig. 10, we show the minimum and maximum ratios themselves, and how they vary with time.

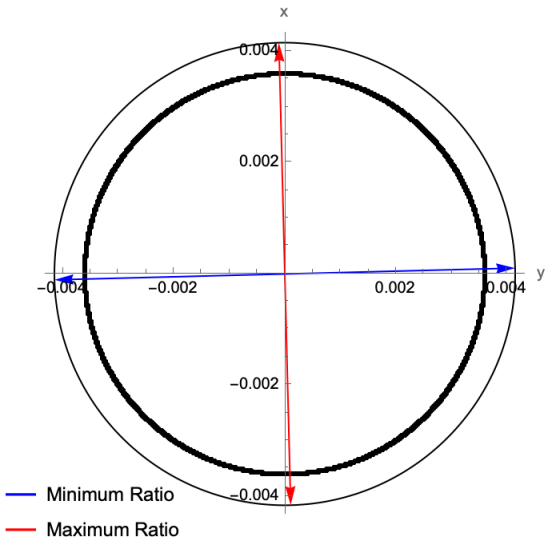

Figure 6: 60 second RRS (km). Energy-limited over-approximation of the fuel-limited RRS is close to uniform in all directions.

We find that the energy-limited reachable set gives a uniformly moderate overestimate of the thrust-limited reachable set for short time of flights. As time of flight increased, we found that the energy-limited RRS improves as an approximation for the thrust-limited reachable-set primarily in the radial direction, while it worsened as an approximation for the thrust-limited RRS primarily in the in-track direction. This is important, because there are parametric methods for generating the thrust-limited reachable set, but finding the range along a particular direction is difficult, while finding the energy-limited reachable set along a particular direction is accomplished very simply.

CONCLUSION

We began by reviewing four types of relative reachable sets under linearized dynamics as well as their computation. We then demonstrated linear algebraic methods employing generalized eigenvalue problems to calculate metrics of interest for comparing impulsive reachable sets with constant-thrust reachable sets to model high-thrust chemical propulsion and comparing energy-limited and thrust-limited reachable sets to model low-thrust propulsion. In the high-thrust case, it was found that the constant-thrust reachable set is rarely a subset and never a superset of the comparable impulsive reachable set. It was also found that the centered RIC frame constant-thrust reachable set is most similar to the impulsive reachable set. Novel analytical forms of the constant-thrust reachable sets were presented to facilitate computations for this analysis.

In the low-thrust case, the thrust-limited reachable set is a more physically meaningful reachable set, but can be time-consuming to compute. On the other hand, the energy-limited reachable set is easier to compute and analyze. It is easy to see that a comparable energy-limited reachable set is always larger than its thrust-limited counterpart. We present new analysis techniques using generalized eigenvalues to describe the position reachable set for an energy-limited scenario and describe the maximum difference in the two reachable sets. We find that the energy-limited reachable set is only ever 1.4 times as large as the thrust-limited reachable set over the course of a period for

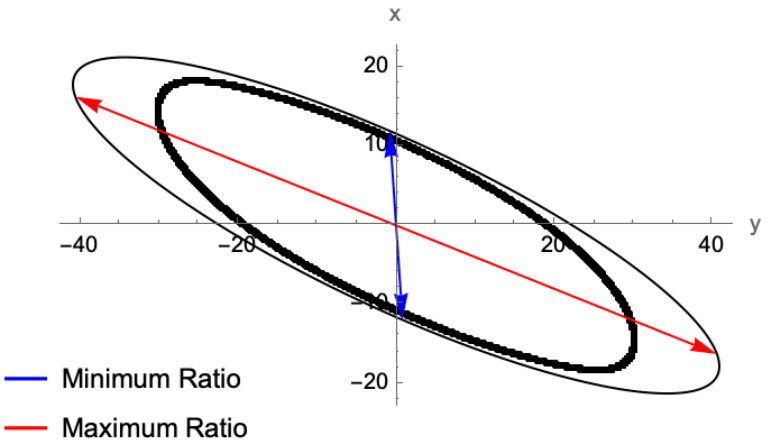

Figure 7: Half Period RRS (km). Energy-limited over-approximation of the fuel-limited RRS is smaller in the radial direction than the in-track direction.

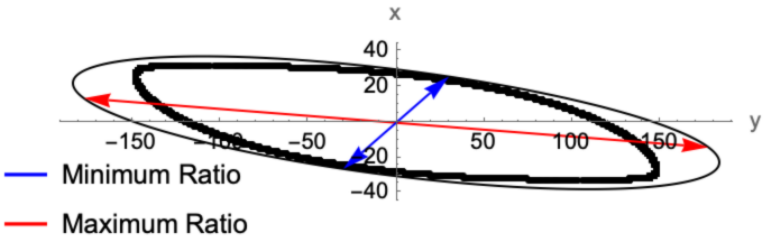

Figure 8: Full Period RRS (km). Energy-limited RRS becomes more accurate as a stand-in for fuel-limited RRS while over-approximating in the in-track direction.

a circular reference orbit, and that along some directions, the energy-limited reachable set is only around a factor of 1.15 times larger than the thrust-limited reachable set. These results may enable future studies to employ the energy-limited reachable set methodology in place of the thrust-limited reachable set methodology when this level of overconfidence–or conservativeness as the case may be–in the reachable set is appropriate for the application.

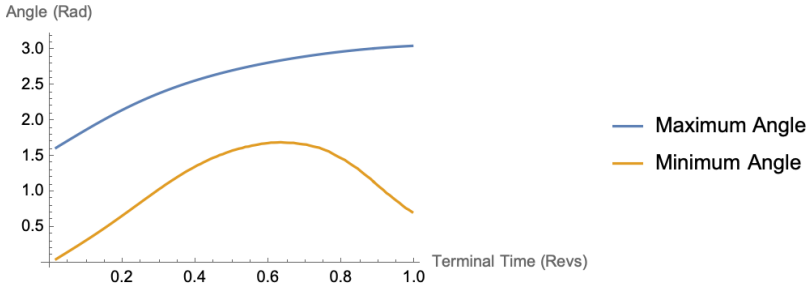

Figure 9: Angles at which the minimum and maximum ratios between RRS occur, as a function of number of revolutions of the reference orbit.

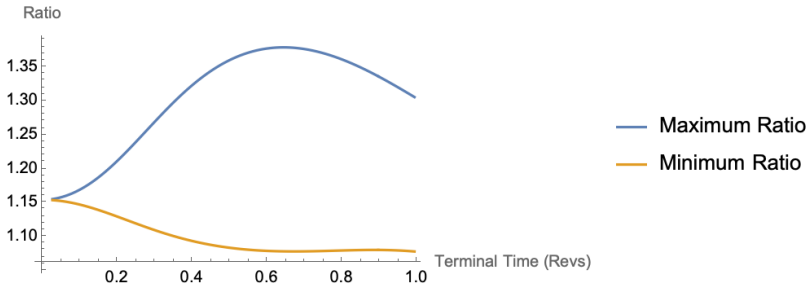

Figure 10: The minimum and maximum ratios between RRS, as a function of number of revolutions of the reference orbit.

REFERENCES

[1] M. Chernick and S. D'Amico, "Closed-form optimal impulsive control of spacecraft relative motion using reachable set theory," *arXiv preprint arXiv:2002.07832*, 2020.

[2] C. Wen and P. Gurfil, "Relative reachable domain for spacecraft with initial state uncertainties," *Journal of Guidance, Control, and Dynamics*, Vol. 39, No. 3, 2016, pp. 462–473.

[3] H. Gong, S. Gong, and J. Li, "Pursuit–evasion game for satellites based on continuous thrust reachable domain," *IEEE Transactions on Aerospace and Electronic Systems*, Vol. 56, No. 6, 2020, pp. 4626–4637.

[4] F. Ankersen, *Guidance, navigation, control and relative dynamics for spacecraft proximity maneuvers*. 2010.

[5] D. Zhou and G. Zhang, "A solution to two-point boundary value problem for power-limited rendezvous with constant thrust," *Acta Astronautica*, Vol. 69, No. 3-4, 2011, pp. 150–157.

[6] S. Lee and I. Hwang, "Reachable set computation for spacecraft relative motion with energy-limited low-thrust," *Aerospace Science and Technology*, Vol. 77, 2018, pp. 180–188.

[7] H. Sun and J. Li, "Analysis on reachable set for spacecraft relative motion under low-thrust," *Automatica*, Vol. 115, 2020, p. 108864.

[8] Z. Wang and F. Jiang, "Analytical Optimal Solution for the Reachable Domain of Low-Thrust Spacecraft," *Journal of Spacecraft and Rockets*, Vol. 61, No. 1, 2024, pp. 274–284.

[9] S. Lizhen, M. Haibin, H. Renhong, and L. Hongjin, "Reachable set estimation for spacecraft relative motion based on bang-bang principle," *Chinese Journal of Aeronautics*, Vol. 36, No. 2, 2023, pp. 229–240.

[10] X. Lin and G. Zhang, "Continuous-Thrust Reachable Set for Linear Relative Motion Near Elliptical Orbits," *IEEE Transactions on Aerospace and Electronic Systems*, 2023.

[11] W. Clohessy and R. Wiltshire, "Terminal guidance system for satellite rendezvous," *Journal of the aerospace sciences*, Vol. 27, No. 9, 1960, pp. 653–658.

[12] K. Yamanaka and F. Ankersen, "New state transition matrix for relative motion on an arbitrary elliptical orbit," *Journal of guidance, control, and dynamics*, Vol. 25, No. 1, 2002, pp. 60–66.

[13] Z. Dang, "New state transition matrix for relative motion on an arbitrary Keplerian orbit," *Journal of Guidance, Control, and Dynamics*, Vol. 40, No. 11, 2017, pp. 2917–2927.

[14] F. J. Franquiz, J. D. Muñoz, B. Udrea, and M. J. Balas, "Optimal range observability maneuvers of a spacecraft formation using angles-only navigation," *Acta Astronautica*, Vol. 153, 2018, pp. 337–348.

[15] L. D. Mullins, "Initial value and two point boundary value solutions to the Clohessy-Wiltshire equations," *Journal of the Astronautical Sciences*, Vol. 40, No. 4, 1992, pp. 487–501.

[16] R. J. Fitzgerald, "Pinch Points of Debris from a Satellite Breakup," *Journal of guidance, control, and dynamics*, Vol. 21, No. 5, 1998, pp. 813–815.

[17] J. Kulik and D. Savransky, "Relative Transfer Singularities and Multi-Revolution Lambert Uniqueness," *AIAA SCITECH 2022 Forum*, 2022, p. 0958.

[18] R. L. Anderson, M. W. Lo, and G. H. Born, "Application of local Lyapunov exponents to maneuver design and navigation in the three-body problem," *AAS/AIAA Astrodynamics Specialist Conference*, 2003.

[19] V. Muralidharan and K. C. Howell, "Stretching directions in cislunar space: Applications for departures and transfer design," *Astrodynamics*, Vol. 7, No. 2, 2023, pp. 153–178.

[20] K. Rivera Lopez and M. Holzinger, "Statistical Analysis of Optimal Stationkeeping Location and Coast Duration Using Stretching Directions," *The Journal of the Astronautical Sciences*, Vol. 71, No. 1, 2024, p. 7.

[21] M. Gu, A. Ruhe, G. Sleijpen, H. Van Der Vorst, Z. Bai, and R. Li, "Generalized Hermitian Eigenvalue Problems," *Templates for the Solution of Algebraic Eigenvalue Problems: A Practical Guide*, pp. 109–133, SIAM, 2000.

[22] A. E. Bryson, *Applied optimal control: optimization, estimation and control*. Routledge, 2018.